

GEOMETRIC DESIGN OF SUPERSONIC RAMJET ENGINES

by

A J Helou, BCE, M.Sc., Ph.D.

July 1995

LIST OF CONTENTS

NOMENCLATURE

CHAPTER 1 INTRODUCTION

1.1 INTRODUCTION

1.2 COMPUTER PROGRAM

CHAPTER 2 THERMODYNAMIC PROPERTIES

2.1 INTRODUCTION

2.2 TWO - DIMENSIONAL SHOCK WAVE

2.2.1 Equations

2.2.2 Mach functions

CHAPTER 3 AERODYNAMIC DESIGN OF DIFFUSER, FLAME HOLDER, COMBUSTION CHAMBER AND EXIT NOZZLE

3.1 INTRODUCTION

3.2 GEOMETRY OF DIFFUSERS

3.3 FUEL MIXING

3.3.2 Ring source injector

3.3.3 Disk source injector

3.4 FLAME HOLDER

3.5 COMBUSTION CHAMBER

REFERENCES

NOMENCLATURE

CHAPTER 2 THERMODYNAMIC PROPERTIES

A	Cross-sectional area
a	Velocity of sound
C_p	Specific heat at constant pressure
C_v	Specific heat at constant volume
G	Flow per unit area or mass velocity = $\frac{W}{A}$
g	Gravity acceleration given to a unit mass by unit force = 32.174 ft/sec ²
k	Ratio of specific heats = $\frac{C_p}{C_v}$
M	Mach number = $\frac{V}{a}$
\bar{m}	Molecular weight
P	Static pressure
\bar{R}	Universal gas constant = 1545.32 $\frac{\text{ft} - \text{lb}}{\text{lb} - \text{mole} - ^\circ \text{Rankin}}$
R	Gas constant = $\frac{\bar{R}}{m}$
r	Pressure ratio
S	Entropy per unit mass
T	Absolute thermodynamic temperature
u	Internal energy per unit mass
h	Enthalpy per unit mass
V	Velocity
v	Specific volume
W	Mass rate of flow
α	Angle between two-dimensional shock and incident flow
ρ	Density
$x = \frac{\rho_y}{\rho_x}$	down stream/upstream flow densities ratio
ω	Wedge angle for two-dimensional shock

Superscript * (asterisk) refers to conditions where $M = 1$

Subscript o (zero) refers to isentropic stagnation conditions

Subscripts x and y refer to conditions upstream and down stream of a shock

NOMENCLATURE

CHAPTER 3 AERODYNAMIC DESIGN OF DIFFUSER, FLAME HOLDER,
COMBUSTION CHAMBER AND EXIT NOZZLE

3.3 FUEL MIXING

E	Edy diffivity, square feet per second
f	Local fuel-air mass ratio (dimensionless)
K	$= \frac{uR_0^2}{4Ex}$ (dimensionless)
M	Radius of a disk source, feet
m	mass of a drop, pounds
P	$= \frac{uM_0^2}{2Ex}$ (dimensionless)
R	Radial distance from survey point to injection source axis, feet
R_0	Radius of ring source, feet
x	Axial distance, feet
u	Average aire velocity, feet per second
W_a'	Air mass velocity, pounds per square feet per second
W_f	Fuel injectionrate, pounds per second
ϕ	Ring source function (see Figure 2, reference 5)
ψ	Disk source function (see Figure 3, reference 5)
$\frac{E}{u}$	Diffusion parameter, feet (see Figure 8, reference 5)

3.4 FLAME HOLDER

V	Velocity of stream past the flame holder, ft/sec
P	Pressure of stream past the flame holder, psi
D	Flame holder effective diameter, inches (see Fig 1(c) & 1(d))
r1	= R/4 Selected arbitrarily (see Fig 1(c) & 1(d))

3.5 COMBUSTION CHAMBER

f	Combustionconcentration exponent
n	Over-all reaction order
P	Pressure, atm.abs.
R	Gas constant. 1.987 gram - ca./((gram - mole)(°K)
T	Reaction temperature, °K
To	Actual inlet temperature, °K

ToE	Effective inlet mixture temperature (T_o corrected for heat loss), °K
V	Reaction volume, liters
x	mole fraction in combustion gases
y	= ϕ for $\phi < 1$; $y = 1$ for $\phi > 1$
ε	Fraction oxygen consumption efficiency
ϕ	Equivalence ratio (fuel/air ratio divided by the stoichiometric fuel/air ratio)

CHAPTER 1 INTRODUCTION

1.1 INTRODUCTION

The ramjet engine is the youngest of the family of jet propulsion devices that includes the rocket, the turbojet and the pulse jet. Because the ramjet depends on its forward motion to achieve compression of intake air, the engine itself employs no moving parts and therefore capable of simplicity and lightness of construction not possible in other air breathing engines. This plus the high thermal efficiency it can achieve, makes the ramjet a favored choice for propulsion of air craft at supersonic speeds.

The principal components of the engine are the inlet diffuser, the fuel distribution device, the flame holder, the combustion chamber and the exit nozzle.

The various problems encountered are solved by studying the following

- a) Thermodynamic properties of air and burnt products of typical hydrocarbon fuels.
- b) Ability to support stable combustion in the wake of baffles.
- c) Correlation of fuel/air ratio stability limits
- d) Prediction of fuel concentration behind injectors
- e) Reaction volume for gaseous system at constant pressure for second order reactions.

The problem considered herein, are limited to the geometric design of the various components of the engine.

1.2 COMPUTER PROGRAM

Based on the information presented herein, a computer program that could be used to optimize the performance of ramjet engines was developed by the author in 1984. The work was published by Hewlett-Packard, 100 N.E. Circle Blvd., Corvallis, Oregon 97330, USA, Series 70 Users' Library, under Category No. J050, Catalogue No. 75001775, in June 19, 1984.

CHAPTER 2 THERMODYNAMIC PROPERTIES

2.1 INTRODUCTION

Air will be treated as an ideally compressible fluid. The effect of viscosity is therefore neglected. The most important consequence of viscosity is probably skin friction due to drag in the boundary layer.

The equation of state for a unit mass of air as well as for many other gases over a range of states which includes most engineering applications is accurately represented by the relations ⁽³⁾

$$Pv = RT \quad (1)$$

$$v\rho = 1 \quad (2)$$

2.2 TWO - DIMENSIONAL SHOCK WAVE

2.2.1 Equations ^(3, 4)

In two dimensional motion the Mach line is represented by a wedge and the lines in which the plane of motion cuts the wedge are Mach lines.

Shock waves can occur at the leading and trailing edges of an airfoil moving at supersonic speeds. The equations relevant to supersonic motion are given as follows

$$x = \frac{\rho_y}{\rho_x} = \frac{\tan \alpha}{\tan(\alpha - \omega)} \quad (3)$$

$$M_x = \left(\frac{5x}{6-x} \right)^{\frac{1}{2}} \csc \alpha \quad (4)$$

$$M_y = \left(\frac{5}{6x-1} \right)^{\frac{1}{2}} \csc(\alpha - \omega) \quad (5)$$

$$\frac{P_y}{P_x} = \frac{6x-1}{6-x} \quad (6)$$

$$P = \rho RT \quad (7)$$

$$V = M\sqrt{kgRT} \quad (8)$$

$$G = \rho V \quad (9)$$

2.2.2 Mach functions ^(3, 4)

$$\frac{T_0}{T} = 1 + \frac{k-1}{2} M^2 \quad (10)$$

$$\frac{\rho}{\rho_0} = \left(1 + \frac{k-1}{2} M^2\right)^{\frac{1}{k-1}} \quad (11)$$

$$\frac{P_0}{P} = \left(1 + \frac{k-1}{2} M^2\right)^{\frac{k}{k-1}} \quad (12)$$

$$\frac{A}{A^*} = \frac{1}{M} \left[\frac{2 + (k-1)M^2}{k+1} \right]^{\frac{k+1}{2(k-1)}} \quad (13)$$

CHAPTER 3 AERODYNAMIC DESIGN OF DIFFUSER, FLAME HOLDER, COMBUSTION CHAMBER AND EXIT NOZZLE

3.1 INTRODUCTION

For the ramjet combustion stability, the fuel/air ratio range of operation is one of most important considerations. Ability to support combustion, seems to be closely related to the rate of heat release in the wake of the baffle. The presence of the baffle provides an extremely low velocity region to which fresh fuel is supplied by re-circulation from the outside stream. When the fresh combustible mixture gives up to incoming mixture the flame blows out.

3.2 GEOMETRY OF DIFFUSERS

Application of simple geometric relations (see Fig 1(a) & 1(b)), the following equations are obtained

$$z = \frac{R - y \tan \alpha}{\tan \omega} \quad (14)$$

$$y = \frac{R \sqrt{1 - \frac{B}{100}}}{\sqrt{\left(\frac{\tan \alpha}{\cos \omega}\right)^2 - \left\{\frac{\cos(\alpha - \omega) \tan \omega}{\cos \alpha}\right\}^2}} \quad (15)$$

where, B is the % blockage of the ramjet clear area normal to the flow of air stream.

3.3 FUEL MIXING

The mixing and distribution of injected liquids in high velocity air streams are of importance in this respect ⁽⁵⁾. Point-source and non-point source solutions are considered in this study.

3.3.1 Point-Source Solution or Diffusion Equation

Equation (16) can be solved for several boundary conditions to give time average fluid concentrations at any point.

$$f = \frac{W_f u}{4\pi W_a' E x} e^{-\frac{uR^2}{4Ex}} \quad (16)$$

(see Figure 8, reference 5 for the determination of E/u)

3.3.2 Ring source injector

For ring source injection, the local fuel/air ratio f , is given by

$$f = \frac{W_f}{W_a' R_0^2} \phi \quad (17)$$

(see Figure 2, reference 5 for the determination of ϕ)

3.3.3 Disk source injector

For disk source injection, the local fuel/air ratio f , is given by

$$f = \frac{W_f}{W_a' M_0^2} \psi \quad (18)$$

(see Figure 3, reference 5 for the determination of ψ)

3.4 FLAME HOLDER

Correlation of fuel-air stability limits with varying pressure, velocity and baffle size was obtained by DeZubay (see Ref. 4 Fig 8 & Ref. 1). The blow-off local fuel-air ratios vs. stability characteristic limits are plotted in Figure 8⁽⁴⁾. Where,

$$\text{Stability characteristic number} = \frac{V}{P^{0.95} D^{0.85}}$$

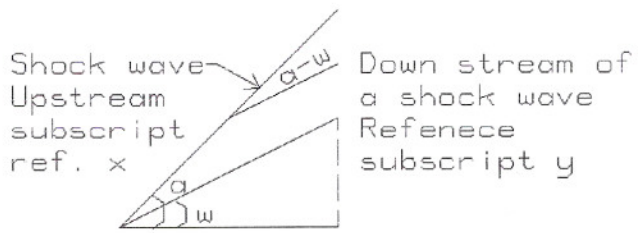
3.5 COMBUSTION CHAMBER

In the design of high output combustion chambers, maximum possible space heat release rates are desired⁽⁷⁾. The eventual limitation on space heat release is the chemical kinetics of the overall combustion reaction. The aim of this article is to minimize the volume and an optimize the design.

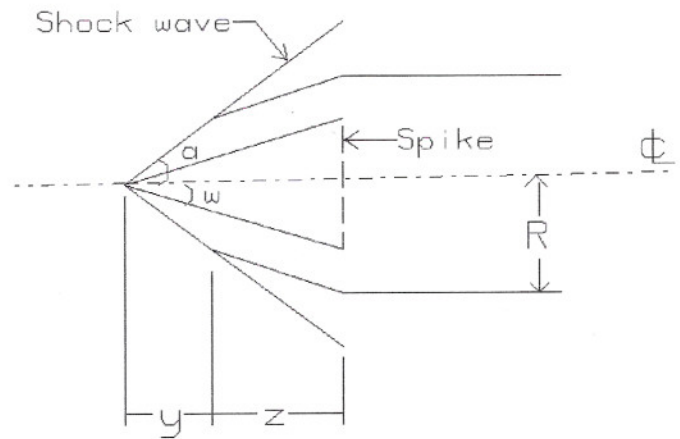
Blowout data correlation for 1.8 order reaction ($n = 1.8$, $f = 0.8$), corrected to 400° K inlet temperature is given in Fig 5 Ref. 7. Equivalence ratio ϕ vs. $\frac{N}{VP^{1.8}}$ data is plotted in this figure.

For inlet temperatures different than 400° K, blowout reaction rates for various effective inlet temperatures relative to ToE = 400° K are calculated in Figure 9 Ref. 7. In this figure, $\left(\frac{N}{VP^{1.8}}\right)_{MAX. AT ToE} \div \left(\frac{N}{VP^{1.8}}\right)_{MAX. AT 400^\circ K}$ vs. $|ToE - 400|^\circ K$ for various equivalence ratio ϕ of lean and rich mixtures, are plotted.

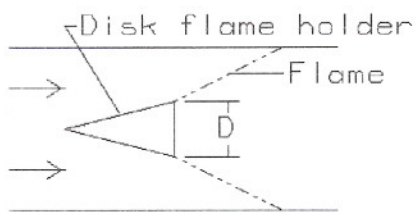
Flame temperatures in ° K for a range of To, ϵ and ϕ of Iso-Octane and dry air at atmospheric pressure are obtained from Table IV Ref. 7.



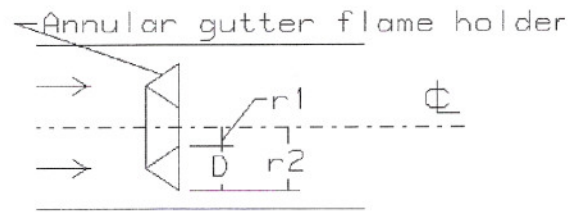
(a)



(b)

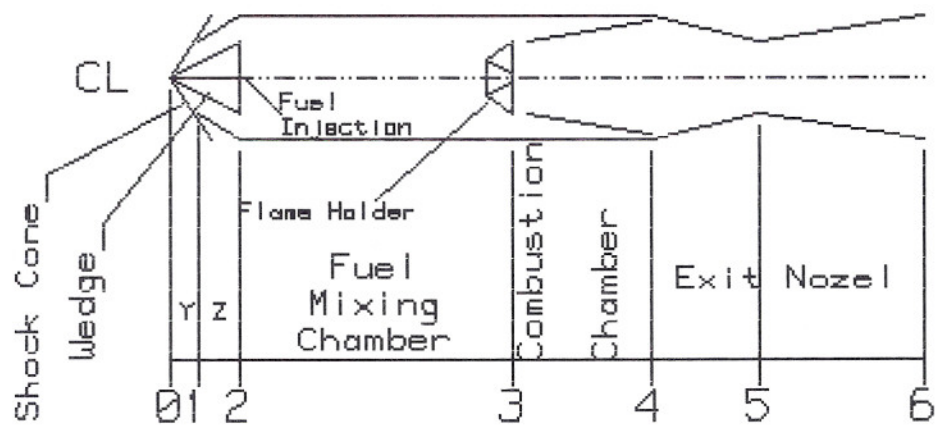


(c)



(d)

Fig 1 Shock waves, diffuser geometry and flame holders cross-sections



Main Components of Supersonic Ramjets

Nomenclature & Abbreviations

A=Cross-sectional Area

D=Density of Flow

G=Mass Rate of Flow

M=Mach Number

P=Absolute Pressure

T=Absolute Temperature

U=Velocity

* Indicates Mach Number=1

Fig 2 Ramjet geometry

REFERENCES

- 1 4th Symposium (International) on Combustion and detonation waves at MIT, USA, 1952
- 2 9th Symposium on Combustion at Cornell University, USA, 1963
- 3 Keenan & Key: Thermodynamic Gas Tables, USA
- 4 Avery, William H.: Twenty - Five Years of Ramjet Development. Reprinted from Jet Propulsion, November 1955. Reprinted from Jet Propulsion, November 1955.
- 5 Longwell, John P. and Malcolm A. Weiss: Mixing and Distribution of Liquids in High - Velocity Air Streams. Standard Oil Development Co., P.O.Box 121 Linden, N.J., USA. Reprinted from INDUSTRIAL AND ENGINEERING CHEMISTRY, Vol. 45 Page 667, March 1953.
- 6 Weiss, Malcolm A., Robert J. Lang and John P. Longwell: Combustion Rates in Spherical Reactors. Esso Research and Engineering Co., P.O.Box 121, Linden, N.J., USA. Reprinted from INDUSTRIAL AND ENGINEERING CHEMISTRY, Vol. 50 Page 257, February 1958
- 7 Longwell, John P. and Malcolm A. Weiss: High Temperature Reaction Rates in Hydrocarbon Combustion. Reprinted from INDUSTRIAL AND ENGINEERING CHEMISTRY, Vol. 47 Page 1634, March 1955.
- 8 Lewis, W. G. E. and M. V. Herbert: AERODYNAMIC FACTORS IN COMBUSTION CHAMBERS.. ENGINEERING August 2, 1957.

to date largely in cut-and-try procedures involving use of an arbitrary number of fuel injection points and variation of the geometrical arrangement and nozzle vaporization characteristics empirically until a satisfactory fuel distribution pattern has been found. Impressive progress has been made, however, in the establishment of engineering design formulas for predicting the rate of fuel spreading from point, disk, and ring sources in a turbulent stream of known intensity (30, 31) and in prediction of the degree of vaporization that will occur in a known time for a particular nozzle type.

Combustor Design

In the development of the first ramjet combustors a major problem was encountered in maintenance of a stable flame in the high velocity flow through the combustor. A solution to the problem was found in the introduction of bluff bodies (baffle flameholders) in the duct, behind which recirculation zones were formed and the flow was sufficiently slow to permit a stable flame to be established. The same result could be achieved by passing the inlet material to the combustor through holes or slots in a perforated plate or cone mounted in the duct. Combustors with the first type of flameholder have come to be called baffle-type combustors, while the latter type are known as "can" combustors.

It was recognized early by the groups at M.I.T. and the Bureau of Standards that a relationship existed between the flameholder dimensions and the flame blow-off velocity, also that the blow-off velocity depended on the fuel-air ratio of the stream impinging on the baffle. Systematic studies of the phenomenon by Scurlock (32) at M.I.T., Longwell (30, 33) at Esso, and DeZubay (34) at Westinghouse showed that blow-off limit at a given fuel-air ratio was approximately proportional to the pressure and effective diameter of the baffle, and inversely proportional to the velocity of flow past the baffle.

The variation of blow-off limit with fuel-air ratio found by DeZubay is shown in Fig. 8. The experimental points indicate the degree of precision of the correlation. Zelinski Rosen, and Walker (35) have shown recently that the DeZubay-Longwell relationship may be improved by a different grouping of parameters and that a similar relationship may be applied to can combustors.

With fuel distribution and stability limits defined in terms of the combustor geometry and air flow, one further major design criterion, heat release rate, is necessary to complete the basic requirements for combustor design. For a given cross-sectional area the latter quantity determines the length of combustor required to achieve a desired combustion efficiency.

It is evident that the heat release rate for a baffle combustor

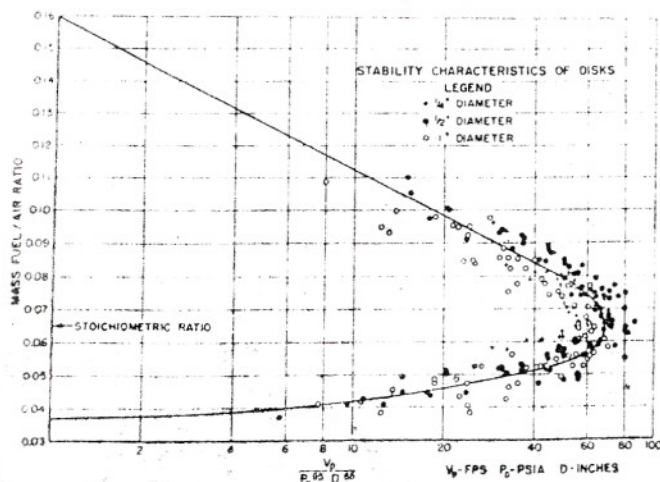


Fig. 8 Stability characteristics of disks

From "Characteristics of Disk-Controlled Flame," by E. A. DeZubay, *Aero Digest*, vol. 61, July 1950, p. 54.

will depend on the rate (or angle) at which the flame spreads into the unburned material from the stabilizing baffles. A combustor length will be required that is somewhat greater than the distance needed for the flame from one baffle to spread to the wall or to come in contact with the flame spreading from another baffle. In a can combustor the unburned material issues into the combustion zone in the form of jets which are gradually consumed. The "jet length" in this case determines the required combustor length.

Several papers have been published on rates of flame spreading from baffles (36), and Zelinski, Matthews, and Bagnall (37) have recently reported the results of a study of the burning rates of confined turbulent jets.

In effect, both baffles and cans may be thought of as devices to introduce sources of ignition from the burned material into the entering combustible mixture. The rate of heat release depends then on the mixing rate and the rate of combustion once an ignition source has been provided. One is led thus to consider types of mixing devices that might lead to maximum heat release rates. This line of reasoning led Avery and Hart to consider what performance might be expected in a combustor in which perfect instantaneous mixing could be achieved (38). They found that definite blow-off limits would exist for such a combustor, defined by the chemical kinetic behavior of the fuel, and that a maximum heat release rate proportional to the square of the pressure for a second-order reaction could be computed. Experimental work by Longwell and Weiss (39) at Esso, who developed a spherical reactor in which very high mixing rates could be achieved, and by the Applied Physics Laboratory group have shown that the theoretical maximum heat release rate for hydrocarbon fuels at normal inlet temperatures is approximately 400 million Btu/atm^{1.8} ft³ hr. The largest experimental value that has been reported for a ramjet combustor is about 20 million Btu/atm² ft³ hr (40). The comparison shows clearly that great gains in heat release rate are possible if more efficient mixing devices than simple cans or baffles can be developed.

Fuel Metering and Control

No published material has been found on fuel metering and control systems for ramjets. However, the requirements of the system are apparent and may be readily outlined. Operation of the ramjet from sea level to altitudes in excess of 60,000 ft will lead to a variation in air flow rate of a factor of ten to fifteenfold. In addition there will be requirement for a two to fourfold variation in fuel flow at a given Mach number and altitude between a lean value for low-drag cruise and a rich value for acceleration and maneuver conditions. Thus the meter must be designed to control fuel flow within, say, $\pm 5\%$ over a fiftyfold variation in total flow. The requirement is a stringent one that leads to a need for precise construction and close tolerances. Intelligence for the speed control may be provided in a number of different ways, the general features of which are readily apparent. For example, fuel rate may be set proportional to ram pressure which is approximately proportional to the air ratio near the design Mach number. Mach number may be determined by the ratio of ram pressure to static pressure and a correction applied to the measured ram pressure to adjust fuel flow to the correct value to cause the vehicle to achieve the desired Mach number. If velocity control is desired, a measurement of the total temperature may be used as a basis for conversion of Mach number to velocity. Mechanical, hydraulic, or electronic servo systems may be employed to achieve the desired accuracy and quickness of response of the control system. The system must, of course, be designed to be insensitive to inertial loads either from the rocket boost or from flight maneuvers. Attention is also necessary to possible effects of aircraft angle of attack on the sensing elements and control requirements, and on the possibility of unstable operation resulting from interaction between the combustor or the diffuser and the metering system.

the intercept equals $W_0/4\pi W_0^2 E z$. Thus, by measuring the distribution downstream of an injection source one can determine if the source behaves as a point. If it does, then the eddy diffusivity can also be directly determined from the slope or intercept or both.

The results of a typical run with contrastream low-velocity injection of Diesel oil through a small tube are illustrated in Figure 7.

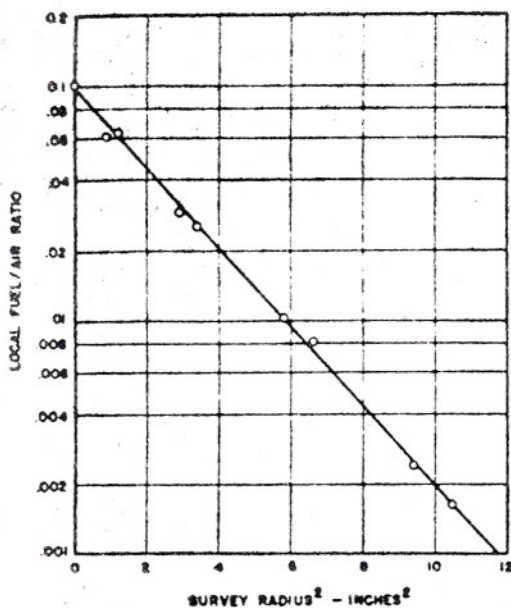


Figure 7. Point Source Injection of Diesel Fuel

For this run, in a 10-inch pipe, air velocity was 200 feet per second at 180° F. and atmospheric pressure. The distribution was measured 34 inches downstream of the source, a tube $1/16$ inch in inside diameter through which fuel was injected at 7.5 feet per second. The data are very well represented by a straight line. In this run as in others cited here, the data are corrected (usually less than 10%) for material balance and for spray asymmetry (usually less than 0.10 inch); the distribution for one half the duct is superimposed on the other half, so that a single average curve can be drawn. From the slope in Figure 7, E calculates to 0.48 square foot per second, and from the intercept, 0.47 square foot per second. Thus it is shown that this injector behaves as a point source and that the diffusivities measured from slope and intercept are consistent.

By means of tests of the type above, the effect on E of several variables was investigated briefly. In some cases, the sources deviated slightly from true point behavior. For these runs, appropriate disk-source corrections were made as described below.

The influence of duct size on E was determined by comparing the distributions obtained in 6- and 10-inch pipes under otherwise identical conditions. Solvent naphtha was injected, at three rates, through a tube $1/16$ inch in outside diameter by $1/32$ inch in inside diameter, 1 inch long. Injection was contrastream to an air velocity of 288 feet per second at atmospheric pressure and 200° F. At a diffusion distance of 35 inches, the following results were obtained:

Fuel Injection Rate, Lb./Sec.	Diffusivity, Sq. Foot/Sec.	
	6-inch pipe	10-inch pipe
0.102	0.55	0.58
0.160	0.55	0.58
0.202	0.55	...

Diffusivity in the 10-inch pipe is only slightly greater than diffusivity in the 6-inch pipe. Data of Towle and Sherwood (9) on gaseous injection in long 6- and 12-inch ducts showed diffusivity to be proportional to duct size, as contrasted to the results here. Confirming their data is the fact that the scale of normal

turbulence in the center of a pipe is, according to Taylor (8), approximately proportional to pipe diameter. Recalling that the diffusivity should be proportional to the scale of turbulence, one would expect the diffusivity to vary directly with pipe diameter.

However, the scale of turbulence is very sensitive to duct length, for short ducts, and to the nature of the flow preceding the section of interest. Therefore, one cannot automatically assume a direct change of diffusivity with duct diameter. This is borne out by the data presented here, in which only a small increase was observed. Some tests under similar conditions in a duct approximately 2 feet in diameter resulted in diffusivities no larger than those observed in the 10-inch pipe. There are two factors responsible for the small effect of duct diameter on diffusivity. (1) The scale of turbulence in these tests probably depended primarily on the upstream perforated plate and not on duct size (as there was insufficient length for normal pipe turbulence to develop). (2) At these high velocities and short diffusion distances, there is enough time for only about one "cycle" of the turbulent air fluctuation. In some cases, time was insufficient for even one cycle. Thus, one would expect scale to be less important than turbulent intensity in determining eddy diffusivity.

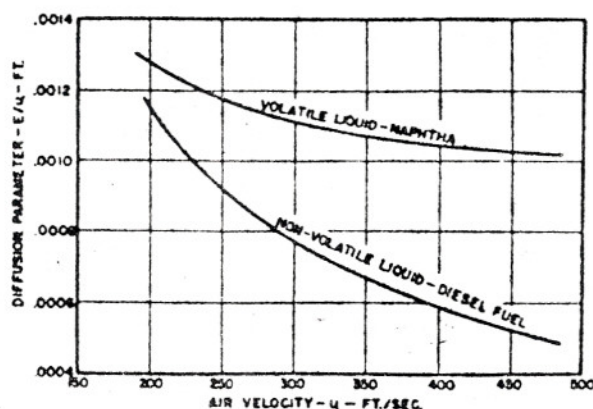


Figure 8. Diffusion Parameter, E/u , for Two Liquids

Data of Little and Wilbur (5) show that the intensity of turbulence (in normal pipe flow) is approximately a constant fraction of the mean flow velocity, u . Because the diffusivity, E , is proportional to the turbulent intensity, one would expect E to vary directly with the flow velocity—i.e., E/u should be a constant. The ratio, E/u , the "diffusion parameter," was determined at several air velocities for point injection of both naphtha and Diesel oil. In these tests, at atmospheric pressure, distributions were measured in a 6-inch pipe 17 inches downstream of the injector. The results, in Figure 8, show that the diffusion parameters approach each other at low velocities but that the parameter for Diesel oil becomes much lower at high velocities. Recalling that the Diesel oil does not evaporate at all, the data show the decrease in diffusivity of liquid drops relative to a vapor (most of the naphtha was evaporated under the test conditions) as velocity increases. This is in accordance with Equation 5, which predicts such a falling off as the frequency of turbulent fluctuation (proportional to average velocity) increases. Some falling off of the naphtha parameter is also evident. This results from the fact that the naphtha is only chiefly, not completely, evaporated. Thus the diffusion parameter is not constant with velocity because of the presence of some liquid drops.

The data of Towle and Sherwood (9) on gaseous injection (of carbon dioxide in air) show some decrease of the diffusion parameter with increasing velocity. In the 6-inch duct, E/u dropped from about 0.0011 to 0.00076 foot when velocity was

tube. Assuming that the injection device does not greatly disturb the flow, the diffusion process and the eddy diffusivity remain the same, so that the differences in distribution must result from the initial conditions. It has been found that for many of the situations encountered in practice, much more of the mixing results from the initial spreading than from eddy transport. Initial spreading must be accounted for as a boundary condition in solutions of the differential equation of diffusion.

POINT-SOURCE SOLUTIONS OF DIFFUSION EQUATION. Equation 1, the basic equation for eddy diffusion, can be solved for several boundary conditions to give time average fluid concentrations at any point. This information is useful for many purposes, but it should be kept in mind that nothing is specified as to instantaneous variations of fluid concentration. Information about variations with time may be required for precisely evaluating the mixing for some combustion purposes. However, time average concentrations have been found useful in most applications.

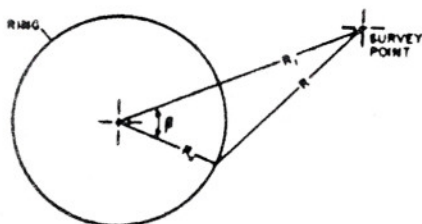


Figure 1. Geometry of Ring Source

A solution to Equation 1 can be obtained by assuming a duct large enough so that wall effects are negligible. Let an air stream flow through the duct with a velocity, u , which is constant at all points. If we assume steady state, a constant, E , and negligible mixing in the mean flow direction, x , compared to mixing perpendicular, r , to the flow direction, then,

$$\frac{\partial f}{\partial x} = \frac{E}{u} \left(\frac{1}{r} \frac{\partial f}{\partial r} + \frac{\partial^2 f}{\partial r^2} \right) \quad (6)$$

by a material balance in cylindrical coordinates. In Equation 6, f is the fuel-air ratio, the local mass ratio of fuel to air. As the injected liquids in this work were always one of two hydrocarbon fuels, the terms "fuel" and "injection liquid" are used interchangeably in what follows. The term f differs slightly from a true fuel concentration. However, it is sufficiently accurate (over the range of interest) for this work and, because of its convenience, is used throughout this report.

A particular integral of Equation 6 can be found using the following boundary condition, a material balance across any section:

$$W_f = 2\pi W' \int_0^\infty f r dr \quad (7)$$

The result is then

$$f = \frac{W_f u}{4\pi W' E x} e^{-\frac{uR^2}{4Ex}} \quad (8)$$

Equation 8 describes the fuel distribution downstream of a point source. R is the radial distance from the survey point (at which the local fuel-air ratio is desired) to the axis of the injection point, and x is the distance, measured along the injection point axis, from the injection point to the survey point. A point-source equation which differs slightly from Equation 8 has been proposed by other investigators—e.g., (9). However, for the range of conditions of interest here, the variation between these equations is usually of the order of a few tenths of 1%; although Equation 8 is not exact, its accuracy is more than adequate here and, in the opinion of the authors, it is considerably simpler to use than the exact equation of (9).

NONPOINT SOURCE SOLUTIONS. It was noted above that a point source is often a very poor approximation to an actual fuel injection device. However, any nonpoint source may be pictured as consisting of an infinite number of point sources properly arranged.

Suppose then that a ring source exists, defining a ring source as a circular line source of radius R_0 ; liquid is injected uniformly

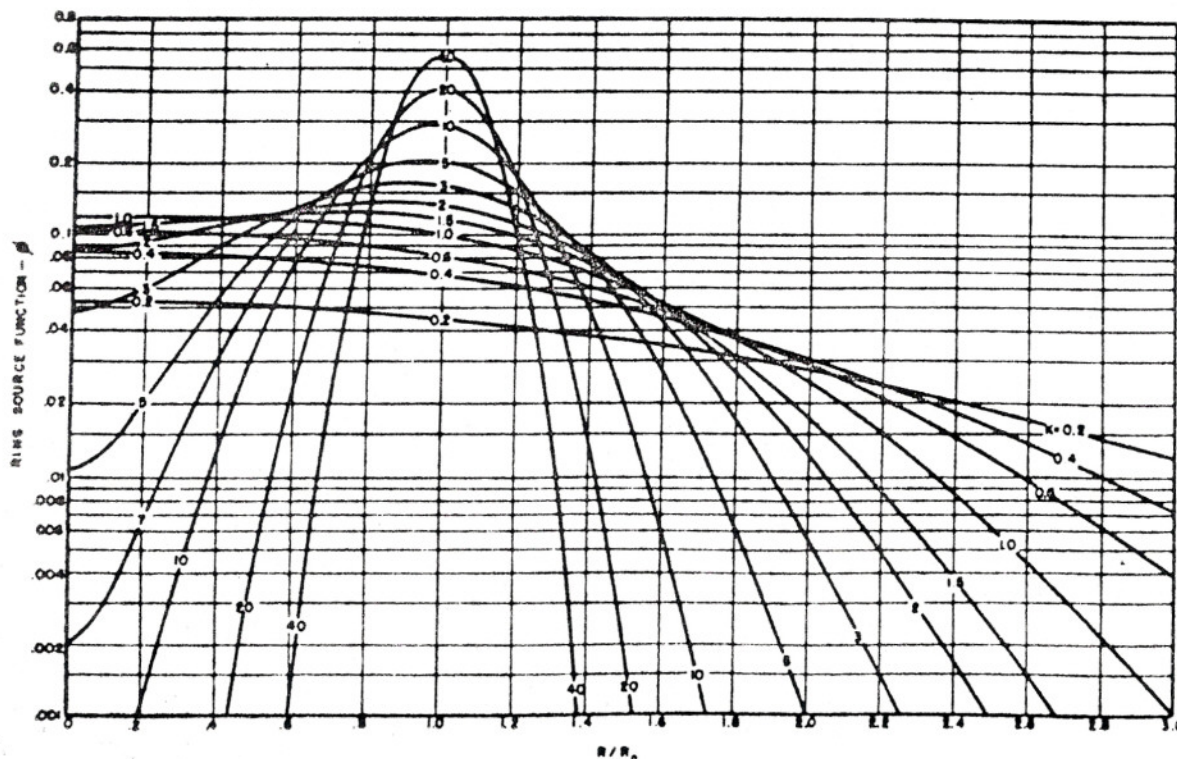


Figure 2. Dimensionless Ring Source Function, ϕ

Ref. 5

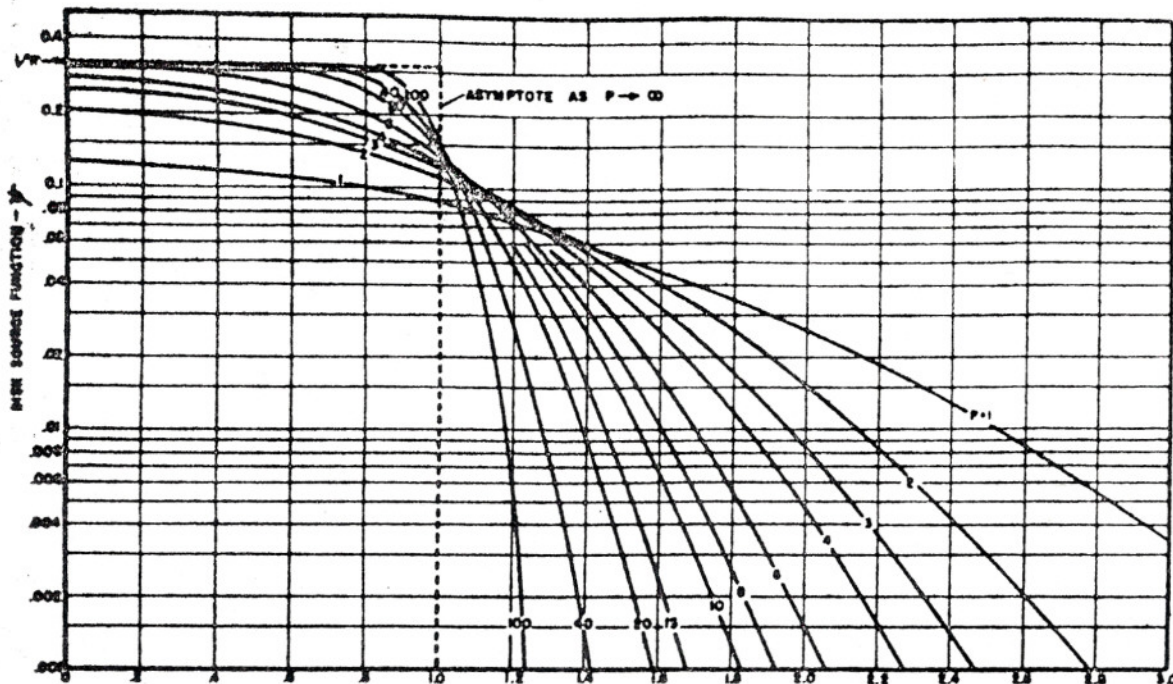


Figure 3. Dimensionless Disk Source Function, ψ R/M

around the ring. This situation can be handled by first assuming that N equal small arcs exist, making up a circle of radius R_0 . If W_f is the total fuel rate to the circle, the rate to each arc is clearly $W_f \Delta\beta / 2\pi$, where $\Delta\beta$ is the angle subtended by each arc. From Figure 1 it can be seen that the distance R varies around the circle but can be given by

$$R^2 = R_1^2 + R_2^2 - 2R_1R_2 \cos \beta = R_2 \left[1 + \left(\frac{R_1}{R_2} \right)^2 - \frac{2R_1}{R_2} \cos \beta \right] \quad (9)$$

As $N \rightarrow \infty$, each arc approaches a point source and the distribution is given by the limit of the following sum:

$$= \lim_{N \rightarrow \infty} \sum_{i=1}^N \frac{W_f \Delta\beta u}{(2\pi) 4\pi W_f' E x} \exp \left\{ \frac{-uR_2}{4Ex} \left[1 + \left(\frac{R_1}{R_2} \right)^2 - \frac{2R_1}{R_2} \cos \beta \right] \right\} \quad (10)$$

This limit is the integral

$$f = \frac{W_f u}{8\pi^2 W_f' E x} \int_0^{2\pi} \exp \left\{ \frac{-uR_2}{4Ex} \left[1 + \left(\frac{R_1}{R_2} \right)^2 - \frac{2R_1}{R_2} \cos \beta \right] \right\} d\beta \quad (11)$$

whose solution is, letting $uR_2/4Ex = K$,

$$f = \frac{W_f K}{W_f' R_2^2 \pi} e^{-K} \left[1 + \left(\frac{R_1}{R_2} \right)^2 \right] I_0 \left(2K \frac{R_1}{R_2} \right) \quad (12)$$

I_0 is a modified Bessel function of the first kind, zero order. The subscript of R_2 has been dropped for convenience between Equations 11 and 12; R is now defined as the radial distance from the axis of any injection source to the survey point. Equation 12 may be simplified to

$$f = \frac{W_f}{W_f' R_2} \phi \quad (13)$$

where ϕ , a function of only the dimensionless groups K and R/R_2 , is plotted in Figure 2. A simple expression, Equation 13, is thus available for the fuel distribution downstream of a ring source.

Specific application of this equation, and the point-source and disk-source equations, is discussed at a later point.

A procedure exactly analogous to deriving the ring-source equation from the point-source equation can be used to obtain a disk-source equation from the ring-source equation.

Assume a disk source to exist, defining a disk source as the entire area bounded by a circle of radius M ; liquid is injected uniformly over the disk area. Consider the area to consist of N annular rings, each of average radius R_0 . Sum up the contribution of each ring as $N \rightarrow \infty$. This procedure gives the integral

$$= \frac{W_f u}{W_f' 2\pi E x M^2} e^{-\frac{uR^2}{4Ex}} \int_0^M R_0 e^{-\frac{uR_0^2}{4Ex}} I_0 \left(\frac{uR_0 R}{2Ex} \right) dR_0 \quad (14)$$

Unfortunately, this integral probably cannot be evaluated in closed form with familiar—i.e., tabulated—functions. However, Equation 14 can be written as

$$f = \frac{W_f}{W_f' M^2} \psi \quad (15)$$

where ψ , a function of the dimensionless groups $P (= uM^2 / 2Ex)$ and R/M , is plotted in Figure 3 from computer-calculated tables. Equation 15 then is a simple expression for the fuel distribution downstream of a disk source.

Although the disk and ring sources are sufficient for this work, it is evident that the above techniques are applicable to sources of any plane geometry.

Experimental Procedures

Mixture Sampling Methods. The performance of a system is influenced not only by distribution, the local mass ratio of injected fluid to air, but by the condition of the fluid—i.e., liquid or gaseous. Two different experimental techniques have thus been used in this work, one for measuring the distribution of liquid fuels (as droplets) and one for measuring fuels which are chiefly gaseous at the measuring station. The former technique, of course, corresponds to injection of a nonvolatile liquid and the latter to injection of a very volatile liquid. The distribution for any intermediate (partially vaporizing) liquid will be somewhere between the volatile and nonvolatile extremes; the intermediate distribution can thus be at least bracketed by the two

Early work suggested that it would be possible to correlate the blowout data by plotting the blowout equivalence ratio against a correlating group of the type N/VP^n , where N is the mass flow, V the reaction volume, P the pressure, and n some unknown pressure exponent. To determine this exponent it is desirable, for a given value of N/VP^n (and thus presumably for a given value of equivalence ratio), to vary N , V , and P independently as widely as possible. Minimum values of V are set by the increasingly large surface-to-volume ratios of smaller spheres. The results would be undesirable increased surface effects and heat losses. The upper limit to V and sphere size is set by laboratory limitations of air supply and exhaust capacity.

The range of blowout pressures for the data of Table II is shown in Figure 3. This range is, of course, conditioned by mass flow limitations in order to maintain a given N/VP^n for a given V . Thus the low pressure limitation is really a minimum mass flow limitation. At lower mass flows, heat losses from the sphere become progressively more important and cause undesirably large corrections. Where 1 atmosphere is not the upper pressure limit, this limit is set by the upper limiting mass flow. Beyond this mass flow, damage to the reactor is so rapid and severe that there is not enough time to obtain useful data. These considerations apply for lean mixtures. Because of poor reproducibility and reactor damage, no attempt was made to investigate thoroughly the rich range.

For these reasons, mass flows in the small reactors were varied from about 0.16 to 2.4 gram-moles of air per second; in the large reactor, extreme values were not attempted and mass flow rates varied from about 2.4 to 6.3 gram-moles per second. In all cases the inlet fuel-air mixture entered at about 400° K. The over-all equivalence ratio range extended from about 0.4 to 2.0.

Equivalence Ratio. All blowout data are tabulated in Table II in order of increasing equivalence ratio. During all runs with lean mixtures a small water-cooled probe (Figure 4) made from three concentric lengths of stainless steel hypodermic tubing was kept in position in the sphere, as shown in Figures 1 and 2. Through this probe, a sample of the combustion gases was withdrawn continuously, compressed by a diaphragm pump, passed through a packed furnace to complete combustion, and then led to an oxygen meter (paramagnetic type). By simple stoichiometry, the residual oxygen in the completely burned gases could be translated to equivalence ratio, ϕ . The ϕ so obtained is the value tabulated in Table II. For rich mixtures, this technique is not applicable without modification, and the ϕ given in Table II was computed from the individual air and fuel rates.

The tabulated air rates were calculated from these equivalence ratios and the known fuel rates; the combined accuracy of oxygen meter and fuel rate was believed to be greater than that of the orifice. However, in all cases the air rate so calculated agreed with the air rate indicated by the orifice meter within a few per cent. The static pressure, P , was that obtained by the pressure tap shown in Figure 1.

The inlet mixture temperature, T_0 , was indicated by thermocouples lying inside the inlet tubes and with junctions at the points where the inlet tubes enter the insulating shell. It should be noted that there is no error due to preheating of the inlet mixture within the inlet tubes and ball (if the latter are within the reaction volume). This heat is simply recycled through the reaction zone—the apparent loss in flame temperature recovered as an equivalent in-

crease in inlet temperature. There is a slight error caused by preheating of the inlet mixture in the section of inlet tube actually passing through the hot firebrick wall. However, this error has been neglected.

Effective Inlet Mixture Temperature. Despite the presence of the insulating shell, there is some heat loss by conduction through the shell. The reactor is nonadiabatic to the extent of this loss. By means of an optical pyrometer, used by sighting through sight port and exit hole, both interior ceramic and exterior nickel average wall temperatures were measured. The observed temperature differential varied from about 250° to 700° K. with absolute interior temperatures to about 2000° K. Heat loss through the brick shell was computed from this differential and the brick thermal conductivity. Values of the latter, supplied by the manufacturer, averaged about 0.002 gram-calories per (second)(cm.)(° K.) in the temperature range of interest. In the equation for spherical conduction, the presence of the exit holes was ignored. These holes occupy between about 10 and 25% of the interior surface area and less than 10% of the exterior surface area. Although some error is thus introduced, it tends to be offset by radiation from the hot walls of the exit holes. There is negligible direct radiation loss from the "bottom" of the hole because, looking along the hole axis, one sees only the relatively cool central injection ball. Once the heat loss has been computed, it is most conveniently expressed as an effective lowering of the inlet temperature; reactor behavior is not influenced by the fact that a given amount of heat is lost by conduction through the walls rather than by being absent from the inlet mixture. Lowering of the effective inlet temperature is directly computed by dividing the heat loss by the product of entering total mass flow and its specific heat.

The variations in reaction volume for a given reactor type (Table I) were chiefly due to small differences in the diameters of the many firebrick shells used. For a given inlet assembly and nickel shell, a dozen or more firebrick liners may have been used. The life of a liner is critically dependent on the conditions of operation. A single liner might last for only one or two runs at high mass flows and near-stoichiometric equivalence ratios. For very lean or very rich mixtures at low mass flows, a liner would remain intact (without fusing or crumbling) for ten or more runs.

Table II also includes the groups correlating mass flow, pressure, and reaction volume corrected to a base of 400° K. inlet temperature. The method of correction from T_{0E} (the effective inlet temperature, the actual inlet temperature minus the effective

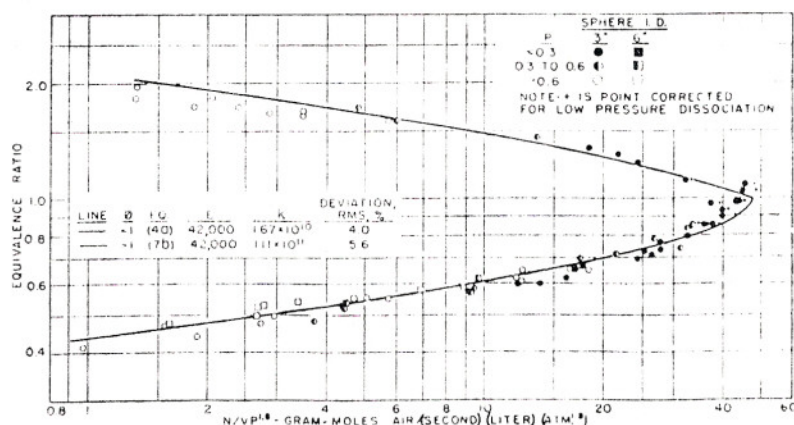


Figure 5. Blowout data correlation for 1.3-order reaction ($n = 1.3, f = 0.8$), corrected to 400° K. inlet temperature

		Equivalence Ratio, ϕ											
		0.4	0.5	0.6	0.7	0.8	0.9	1.0	1.0	1.1	1.2	1.5	2.0
$N/VP^{1.3}$	ϵ	0.539	2.82	8.92	19.3	32.6	43.7	48.0	48.0	35.6	26.8	9.13	1.57
	T	0.94	0.93	0.92	0.91	0.89	0.87	0.83	0.75	0.76	0.77	0.78	0.81
		1315	1490	1655	1800	1915	2010	2035	1995	1940	1800	1713	14.70

Ref. 7

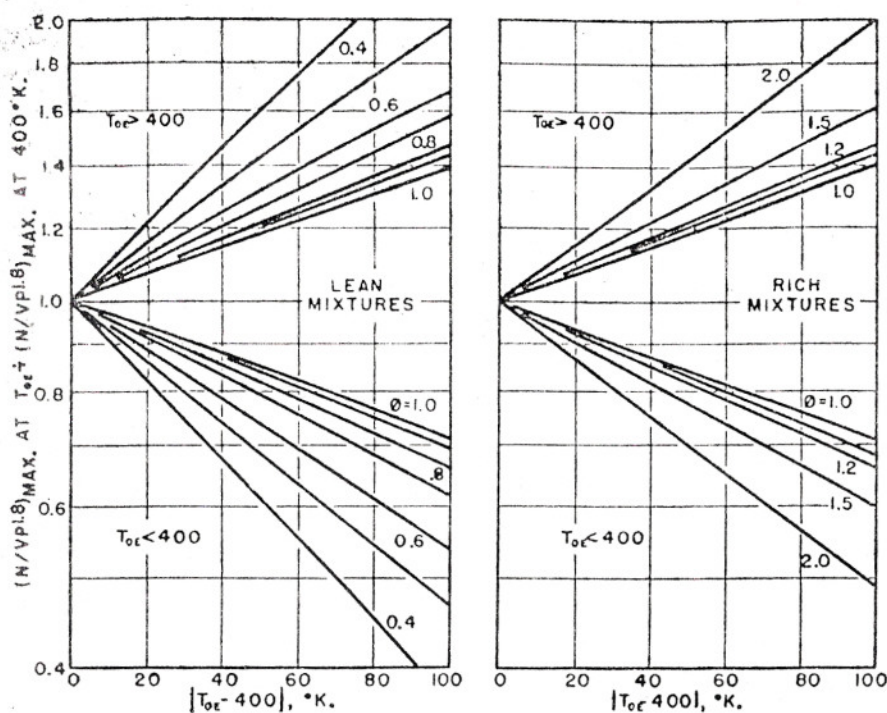


Figure 9. Calculated blowout reaction rates for various effective inlet temperatures

Relative to rates at $T_{0E} = 400^\circ \text{K.}$
Equations and constants as shown in Figure 5

By using $f = 0.8$ in Equation 4a, the lean data were best correlated with an E of 42,000 calories per mole. The same f and E were used in Equation 7b to fit the rich data of Figure 5. Computed values of $N/VP^{1.8}$, ϵ (within 0.01), and corresponding T are tabulated in the caption of Figure 5. Differences in k result from the different assumptions as to the nature of the combustible and the combustion gas composition for the lean and rich mixtures. The semitheoretical curves computed from these constants are shown in Figure 5. The data points near $\phi = 1$ in Figure 5 (and Figure 10) were obtained at relatively high temperature and low pressure. Dissociation corrections to reaction temperature at these low pressures are greater than those incorporated in the atmospheric pressure temperatures of Table IV. Thus the temperatures are lower and reaction rates correspondingly lower. The semitheoretical curve reflects the data corrected to atmospheric pressure reaction temperature, thus eliminating this extra dissociation effect at low pressure. This correction did not exceed 8% in $N/VP^{1.8}$ at any point. Reduction in flame temperature at low pressures is illustrated by the following Bureau of Mines calculations (2) for $\text{C}_{10}\text{H}_{20}$ fuel at $T_0 = 400^\circ \text{K.}$ and $\epsilon = 1.0$:

P	Flame Temperatures, $^\circ \text{K.}$, at Equivalence Ratio, ϕ				
	0.667	0.818	1.000	1.222	1.500
1.000	1935	2177	2350	2313	2119
0.398	1933	2163	2317	2297	2115
0.158	1929	2146	2282	2275	2110
0.100	1926	2136	2263	2263	2107

Once the values of the kinetic constants in Equations 4a and 7b have been established, the blowout values of $N/VP^{1.8}$ and ϕ can be recomputed for various inlet temperatures. An inlet temperature other than 400°K. implies only a different T for a given ϵ in the equations. The blowout $N/VP^{1.8}$ for a given ϕ can then be compared, for various T_{0E} , to the blowout value for the same ϕ at $T_{0E} = 400^\circ \text{K.}$ This has been done in Figure 9, using the kinetic constants of the curves of Figure 5. Figure 9 was used in Table II to correct the blowout rates to 400°K. for effective inlet temperatures other than 400°K. It is clear from this figure how

heat losses affect the blowout rates in reducing total enthalpy; the enthalpy loss is accounted for by an equivalent decrease in inlet temperature.

Equation 4a was also used, with these same constants, to predict the dot-dash curve of Figure 8. Values of ϵ from about 1.0 to 0.9 were simply substituted with the corresponding T , to obtain the curve. Although the data points fall below most of the curve, the efficiencies at blowout are in reasonable agreement.

In any case, the correspondence of ϵ for given $N/VP^{1.8}$, regardless of individual values of N and P , lends credence to the reaction rate concept. The exact level of predicted efficiency depends on the reactants assumed. For example, if oxygen were reacting with C_3H_8 rather than carbon monoxide—thus requiring the use of Equation 7a rather than Equation 4a—agreement between observed and predicted efficiencies would be excellent.

OBSERVED SPACE HEAT RELEASE RATES ARE VERY HIGH

The maximum value of $N/VP^{1.8}$ of Figure 5 (dissociation corrected) is about 48. Equation 4a predicts that the combustion efficiency is 0.83. This rate of

reaction corresponds to a space heat release rate of about 3.0×10^8 B.t.u. per (hour) (cubic foot) ($\text{atm.}^{1.8}$). Such a rate is an order of magnitude greater than the highest published experimental value (11) for an appreciable volume known to the authors. Lack of other data makes direct comparison of these results impossible. This rate will not necessarily correspond to the previously discussed highest local rate appearing in laminar flames. In a laminar flame, it is certainly possible that a happy combination of heat and mass diffusions may give a local combination of temperature and reactant concentrations that results in a rate higher than observed here.

In previous theoretical treatments of homogeneous combustion (1, 3, 9, 14, 16), it was assumed that the over-all reaction order was 2.0 with equal combustible and oxygen exponents. If such assumptions are made in this case, the data can be plotted as shown in Figure 10. However, there is a pressure trend in the lean data points—lower pressure points fall below and to the right. The solid curve best fits the lean data with Equation 4a using $E = 42,000$ and the rich data with Equation 7b and the same E . The most significant deviations again occur for very rich mixtures where the data are most questionable.

If the further usual assumption is made that the combustible material is original fuel (rather than carbon monoxide), Equation 7a is used for the lean data. Thus the dotted curve of Figure 10 was calculated with a best-fitting E of 40,000 and this same E in Equation 7b for rich mixtures. The fit here is poorer, particularly near $\phi = 1$.

For both curves, k was chosen for the rich mixture equation so as to make N/VP^2 at $\phi = 1$ coincide for both lean and rich branches. All of the data of Figure 10 were corrected to a 400°K. inlet temperature reference by using Figure 9. Figure 9 is negligibly in error for small variations in E , n , or f .

Although use of N/VP^2 with $f = 1$ is a slightly more convenient approximation, it predicts somewhat optimistic heat releases (at pressures higher than the pressures used). Thus, the maximum observed N/VP^2 is 74 (corrected for low pressure dissociation), and the maximum values predicted by the two curves are 68.5 and